

A New Algorithm for Innervation Zone Estimation Using Surface Electromyography: A Simulation Study Based on a Simulator for Continuous sEMGs

Malte Mechtenberg^{1,2}^a, Nils Grimmelsmann^{1,2}^b and Axel Schneider^{1,2}^c

¹*Biomechatronics and Embedded Systems Group, University of Applied Sciences and Arts, Bielefeld, NRW, Germany*

²*Institute of System Dynamics and Mechatronics, University of Applied Sciences and Arts, Bielefeld, NRW, Germany*

Keywords: Innervation Zone, Muscle, Innervation Point, EMG, EMG Simulation, Electromyography, Motor Unit, Firing Pattern, EMG Array.

Abstract: In this work, a novel algorithm for the estimation of the innervation zone location within a muscle head is presented. The algorithm is able to identify innervation zone clusters within continuous surface electromyography (sEMG) recordings based on linear electrode arrays. The presented algorithm is tested in a simulation environment, which is capable of simulating EMG signals based on a common drive signal (activation). The simulator was used to generate sEMGs of six virtual muscle based on six different configurations for the respective muscle fibre distributions. The virtual muscles were each activated with a trapezoidal signal (common drive). The new algorithm was able to identify the location of the innervation zone centers with a mean absolute error of 3.8% of the inter electrode distance. In the best case, the absolute error was below 1% of the inter electrode distance.


1 INTRODUCTION


This work introduces a new algorithm for the estimation of innervation zones in an electromyography recording. It is based on a previously published algorithm (Mechtenberg and Schneider, 2023) that was only able to find one innervation zone location per EMG recording, thus requiring manual labor when multiple innervations zone locations have to be identified in a recording. The novel extension presented here allows an automatic detection of multiple innervation zone locations within one recording. Thus being comparable to other methods presented in the literature, that are for example (Mesin et al., 2009; Beck et al., 2012; Marateb et al., 2016; Huang et al., 2023). The method presented here has a small parameter set and an implementation that is available as open source software (Apache 2.0 license) (Mechtenberg, 2023b).


A Brief Introduction to Innervation Zones. Muscle fibres of skeletal muscles are controlled by so-called motor neurons which are situated in the pe-

ripheral nervous system within the spine. A motor neuron connects to several muscle fibres. The combination of muscle fibres and a motor neuron is called a motor unit. An axon of a motor neuron connects to the respective muscle fibre at the so-called innervation points (IPs) via the motor end plates. The innervation points of a motor unit are distributed over the muscle body. This distribution of IPs is called the innervation zone (IZ) of the motor unit. The IZ locations vary considerably between subjects (Guzmán et al., 2011). Moreover, during contraction, the length and position changes of the muscle also change the relative position of the IZs (Piitulainen et al., 2009; Martin and MacIsaac, 2006).

In summary, the IZ location is specific for a subject and experiment condition. This means it is hard to follow heuristics, based for example on anatomical measures to localize the IZ. An attempt was made with an atlas of innervation zones (Barbero et al., 2012). This atlas is considered as a general reference for the distribution of IZs between multiple subjects. It is, however, lacking when precise knowledge of the innervation zone is needed, as for example in the following scenarios.

^a <https://orcid.org/0000-0002-8958-0931>

^b <https://orcid.org/0000-0002-4864-4978>

^c <https://orcid.org/0000-0002-6632-3473>

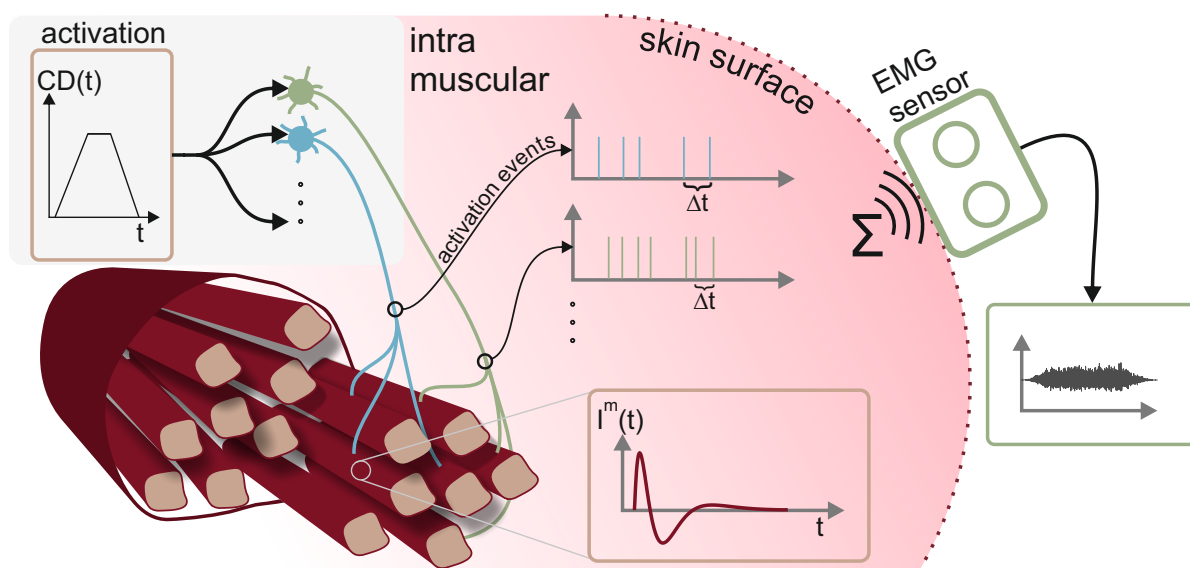


Figure 1: Representation of a motor unit pool consisting of several motor units (green and blue) that are triggered by a common drive (CD) signal (trapezoidal, top left). The times between individual firing events (Δt) are drawn from normal distributions with the corresponding mean frequency and standard deviations as described in eqs. (1) and (2). The simulator determines the measurable potentials on the skin surface (EMG sensor, top right) from the temporal course of all firing events (respectively the corresponding spread of the motor unit action potentials on the muscle fibres).

Possible Applications of Precision IZ Location Estimation. The precise localization of innervation zones is of interest for example in:

- medical treatments, when drugs have to be delivered close to the motor end plates (Zhang et al., 2016).
- exoskeletal control the observed IZ movement could be used as a measure for the amount of muscle shortening (Mechtenberg and Schneider, 2023).
- case of sEMG acquisitions where a consistent signal quality is required over a wide range of movements and subjects. As the sEMG signal characteristics are different when the recording electrodes are placed close to innervation zones compared to locations above the muscle fiber with no IZ or muscle fiber end close by.

In general, an accessible and reliable algorithm to identify the IZ *in situ* could help to improve experimental setups involving sEMG recordings.

Over the years, different methods to estimate the innervation zone location based on sEMGs emerged. An experienced experimenter is able to detect the IZs by visual sEMG inspection. There were multiple attempts to automate this process with signal processing algorithms (Mesin et al., 2009; Beck et al., 2012; Marateb et al., 2016). However, these algorithms require the selection of appropriate param-

eter sets. Tuning them appropriately can be challenging. Mechtenberg and Schneider proposed a new algorithm for the innervation zone detection which uses only two parameters. In a simulation study, an optimization of these two parameters was performed successfully under varying noise conditions (Mechtenberg and Schneider, 2023). In that study, the algorithm operated only on a single motor unit potential, i.e. the EMG signal generated by the sum of all action potentials that travel along the muscle fibres of their respective motor unit. An sEMG recording usually consists of several motor unit potentials generated from different motor units. In order to use the proposed algorithm to estimate the innervation centre in more realistic scenarios (with multiple motor units and activation events), the algorithm needs to be extended. To test this extension, Mechtenberg and Schneider’s simulator (Mechtenberg, 2023a) must also be modified to simulate the activation of many motor units, resulting in a continuous sEMG. Both, the extension of the algorithm and of the simulation framework are subject of this work.

The simulator extension is described first in section 2.1. The experimental setup is then described in section 2.2 before the extension of the innervation zone estimation algorithm is described in section 2.3.

The presented algorithm achieved a mean absolute error of 0.19 mm ($SD(AE) = 0.19$ mm), that is 3.8% of the inter electrode distance.

2 METHODS

2.1 Extension of the EMG Simulator Using the Motor Unit Pool Model

As a basis for the EMG simulation, the approach described in (Mechtenberg and Schneider, 2023) was used. That simulator was only capable of simulating single motor unit potentials. This means, that several motor units were only triggered once in the simulation. It was therefore expanded to include the capability of generating a continuous EMG signal based on a continuous muscle activation signal (the common drive). The concept is depicted in fig. 1. It is similar to the approach that was described by (Petersen and Rostalski, 2019). Here, it was assumed that motor units are organized in a pool. Such a motor unit pool is assumed to receive a common activation signal the *common drive* (CD). The common drive signal is always between zero and one, where zero corresponds to no activation and one is the full activation of a motor unit pool. Each motor unit within a pool is assumed to start firing from a distinct common drive level $CDS_{i_{MU}}$ that is unique for each motor unit i_{MU} . The value of $CDS_{i_{MU}}$ follows the size principle as described later in this section (see also eq. (3)).

When the i^{th} motor unit is active, it generates action potentials with a mean firing frequency $\tilde{f}_{i_{MU}}(\text{CD})$ that is dependent on the common drive level. The relationship of the mean firing frequency to the common drive is modeled utilizing eq. (1) as described by (Petersen and Rostalski, 2019):

$$\tilde{f}_{i_{MU}}(\text{CD}) = \begin{cases} \begin{cases} -[c_2 - \text{CD}] \\ \cdot c_1 \cdot CDS_{i_{MU}} \\ + c_3 \cdot \text{CD} + c_4 \\ -[c_5 - c_6 \cdot \text{CD}] \\ \cdot e^{-\frac{\text{CD} - CDS_{i_{MU}}}{c_7}} \end{cases} & \begin{matrix} CDS_{i_{MU}} \leq \text{CD} \\ \text{CD} \leq 1 \end{matrix} \\ \text{undefined} & \text{otherwise} \end{cases} \quad (1)$$

The actual firing events are generated according to algorithm 1. Once the common drive CD reaches the starting common drive level $CDS_{i_{MU}}$ of a motor unit, the time difference of the next firing instance to the current instance of this motor unit is drawn from a normal distribution. The mean of that distribution is defined by $\tilde{f}_{i_{MU}}(\text{CD})$ (see eq. (1)). The standard deviation of the normal distribution according to (Petersen and Rostalski, 2019) is

$$\sigma_{f,i_{MU}}(\text{CD}) = \frac{10 + 20 \cdot \exp\left(-\frac{\text{CD} - CDS_{i_{MU}}}{2.5}\right)}{100 \cdot \tilde{f}_{i_{MU}}(\text{CD})} \quad (2)$$

Result: motor unit activation pattern
 $t := \text{time_span.start};$
while $t \leq \text{time_span.end}$ **do**
 $\text{CD} := \text{CD}(t);$
 if $\text{CD} \geq CDS_{i_{MU}}$ **then**
 $\Delta t := \mathcal{N}\left(\frac{1}{\tilde{f}_{i_{MU}}(\text{CD})}, \sigma_{f,i_{MU}}(\text{CD})\right);$
 add activation event at $t + \Delta t$
 else
 $\Delta t := 10^{-5};$
 end
 $t += \Delta t;$
end

Algorithm 1: Activation pattern generation of the i^{th} motor unit.

Employment of the Motor Unit Size Principle.

All motor unit parameters, which are not related to the muscle geometry are assumed to be depended on the motor unit size. Here, the motor units are ordered by size, i.e. the smallest motor unit has an index of $i_{MU} = 0$ and the largest of $i_{MU} = N_{MU}$. N_{MU} is the amount of all motor units in the simulated muscle. This assumption is commonly known as motor unit size principle. The motor unit parameters that depend on the motor unit size are the mean conduction velocity, number of muscle fibres within a motor unit and the common drive threshold $CDS_{i_{MU}}$. The relation of the first two motor unit parameters are described in (Mechtenberg and Schneider, 2023). The latter is parameterized by the description of (Petersen and Rostalski, 2019), which is an adoption of the motor unit pool model described by (Fuglevand et al., 1993).

$$CDS_{i_{MU}} = \exp\left(\frac{\log(100 \cdot \text{CDMax}_{i_{MU}}) \cdot i_{MU}}{N_{MU}}\right) \quad (3)$$

Where $\text{CDMax}_{i_{MU}} = 1$ was chosen as the the maximal common drive for a given motor unit.

After the generation of the motor unit firing events the motor unit potentials are simulated once per motor unit. Afterwards a motor unit potential train is generated by shifting the motor unit potentials to the generated firing events. This shift is done in the discrete time domain. Therefore, the motor unit potentials can not be shifted to the exact time point of each firing event. Instead, the potentials are shifted to the discrete point in time that is closest to the respective firing event. The time resolution is set to the time step size $T = 0.05$ ms used during the motor unit potential simulation.

In a last step, all instances of motor unit potentials are summed up at each electrode location and down-sampled to $f = 2$ kHz.

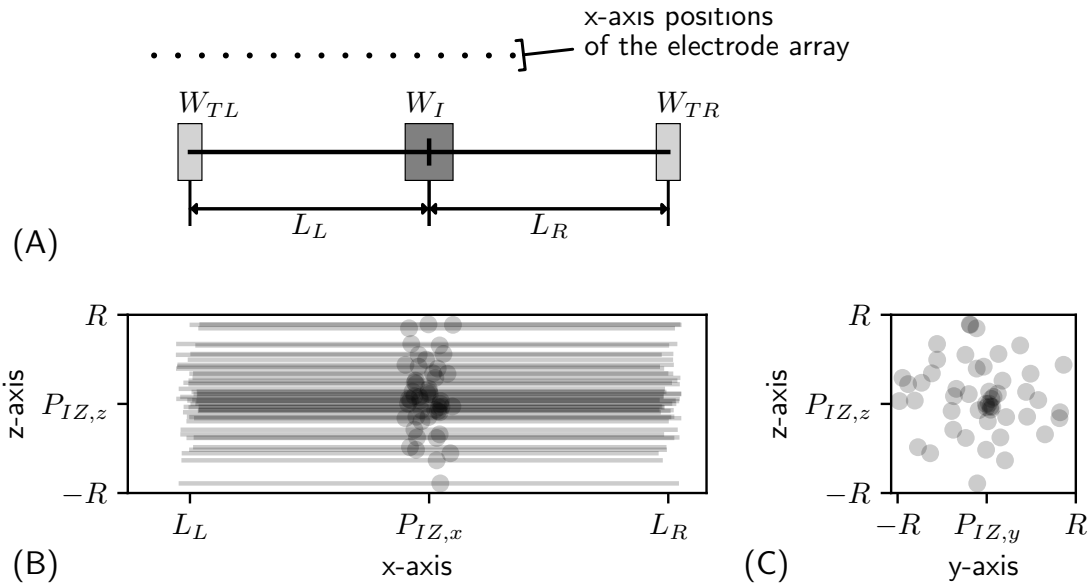


Figure 2: (A) Schematic depiction of the muscle shape defining parameters in the x-axis direction. W_{TL} and W_{TR} are the width of the tendon placement regions on the left and right side of the muscle. L_L and L_R are the distances between the center of the innervation zone and the centers of the two tendon regions. The parameter W_I defines the width of the innervation zone of the muscle. The location of the motor end plate (innervation point IP) as well as the left and right myotendinous junctions in the x-axis are drawn from a uniform distribution in these regions. The relative position in the x-axis of the electrodes is also shown as black dots in the top part. (B, C) depict 50 muscle fibres generated from the setup in (A), where the z- and y-coordinates of the innervation points are drawn from a uniform circular shaped distribution with the radius R around the center of the innervation zone. The innervation points are marked with a black dot. The muscle fibres are drawn with a transparency.

2.2 Setup of the EMG Simulation

The simulator in this study can in principle generate virtual muscle fibres of motor units with different lengths (L_L, L_R), sizes of the innervation zones (W_I) and sizes of tendon regions (W_{TL}, W_{TR} , location of the junction from muscle fibre to tendon) as shown in fig. 2 (A). These five parameters are called *shape defining* parameters. The muscle fibres can be distributed across a spatial volume with the help of their *position* parameters ($R, P_{IZ,y}, P_{IZ,z}$, see fig. 2 (B, C)). For details of the *shape defining* and *position* parameters of the muscle fibres see (Mechtenberg and Schneider, 2023).

In this study, two scenarios were simulated. Scenario I is displayed in fig. 3 (A) and scenario II in fig. 3 (B). The *shape defining* parameters and the *motor unit pool recruitment related* parameters are set to the same values for both scenarios. All constant parameters are listed in table 1 in the appendix.

In Scenario I, the muscle shape related parameters $W_I, W_{TL}, W_{TR}, L_L, L_R$ are kept constant. But the location of the whole muscle was shifted along the x-axis relative to the electrode array (see fig. 3 (A)).

$$P_{IZ,x} \in \{5.75 \text{ cm}, 4 \text{ cm}, 1.75 \text{ cm}\} \quad (4)$$

This way, different innervation zone locations can be tested with a varying influence of the end effect, that occurs at the myotendinous junction.

In Scenario II, the muscle shape related parameters L_L, L_R and the innervation zone center along the x-axis were varied. The remaining parameters were kept constant. L_L and L_R were chosen such that the myotendinous junctions remain at the same position left and right of the electrode array, as displayed in fig. 3 (B), while the innervation zone locations were set to eq. (4).

The virtual electrode array was always placed at the same position for all scenarios. The electrode array consists of 16 monopolar electrodes with a 5 mm spacing. All electrodes had the same y- and z-coordinates (table 1). The first electrode in the array is placed at $x = 0$ cm.

The result of the simulation is a monopolar recording from a continuous simulated EMG for each muscle based on a trapezoid common drive signal. The common drive signal that was used is shown in fig. 4.

For the later use of the EMG signal in the algorithm for innervation zone center estimation, the monopolar recording was converted into a double dif-

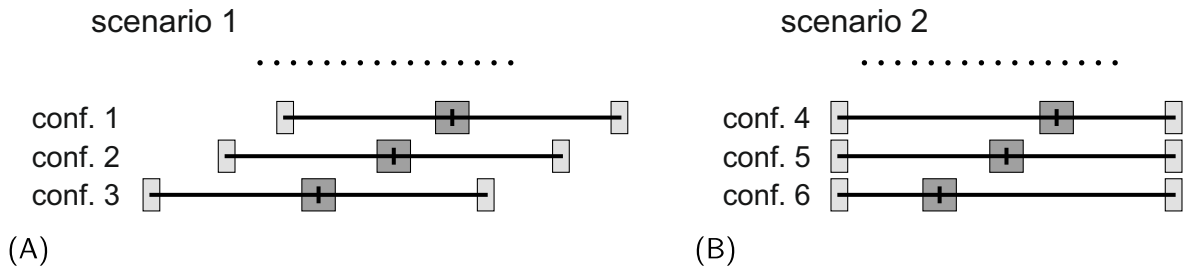


Figure 3: Depiction of the innervation zone and myotendinous junction centers of each simulated virtual muscle relative to the x -axis position of the electrode array. Two types of innervation zone position shifts were simulated. In (A) the innervation zone location relative to the virtual muscle stays the same, but the virtual muscle as a whole is shifted along the x -axis relative to the electrode array. In (B) the myotendinous junction centers remain at the same position on the x -axis, but the innervation zone centers are shifted relative to the electrode array. In total, six muscle configurations were simulated, all with the same muscle belly radius R and with the same y -, and z -axis coordinates for the innervation zone center.

ferential recording as described in (Mechtenberg and Schneider, 2023), resulting in 14 double differential (DD) EMG signals.

2.3 Innervation Zone Center Estimation

As a basis for the innervation zone center estimation, the algorithm introduced in (Mechtenberg and Schneider, 2023) was used. That algorithm operates on a time window of the EMG signal and is able to find one estimation of the innervation zone center per time window. The algorithm basically consists of two steps.

Step 1. Per double differential electrode potential (one of the above-mentioned 14 DD-signals), one motor unit potential (MUP) is identified using a wavelet correlation. This step is parameterized with the wavelet width λ . As wavelet, the third Hermite-Rodriguez series expansion was selected, as this was proposed by (Farina et al., 2000) for the identification of double differential MUPs. After identification of the motor unit potentials in each of the DD-signals, the algorithm uses pairs of any combination of two of those potentials to set up a linear extrapolation (line) that represents the location of the MUPs at earlier points in time. Since the MUPs travel in both directions away from the innervation zone, the intersection of those extrapolated lines of MUPs that travel in one direction and those of MUPs that travel in the other direction represent the innervation zone.

Step 2. The intersection points are clustered using the density based DBSCAN algorithm (Pedregosa et al., 2011). The cluster that contains the largest number of intersections is used to calculate the innervation zone center location estimate, i.e. the center of that cluster. This step is parameterized with

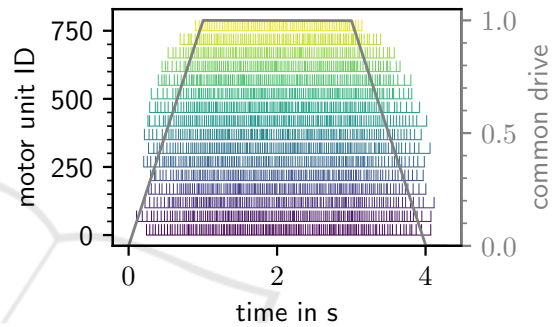


Figure 4: The activation patterns for every 50th motor unit within a virtual muscle are shown, with the corresponding common drive signal that was used to generate the activation patterns (trapezoidal shape). The color of the firing events encodes the motor unit size, which also becomes bigger with increasing motor unit ID i_{MU} .

the density parameter ϵ of the DBSCAN algorithm.

The result of these two steps is a position relative to the x -axis of the electrode array and a point in time. In the previous study (Mechtenberg and Schneider, 2023), a parameter variation was performed in order to find a suitable parameter set, which is tolerant to noise but still accurate. Based on that work, the parameters $\lambda = -0.00391667$ and $\epsilon = 1.10083333$ were selected. For details on the internal parameters please refer to the publication (Mechtenberg and Schneider, 2023) or the open source implementation of the algorithm (Mechtenberg, 2023b).

Extension to Estimate Innervation Zone Centers in Continuous EMG Recordings.

In this study, the algorithm described above was extended to operate on a continuous EMG signal. This extension contains two aspects.

First, the continuous EMG had to be segmented into multiple time windows. For that, a 40ms Hann window was used. The Hann window reduces the

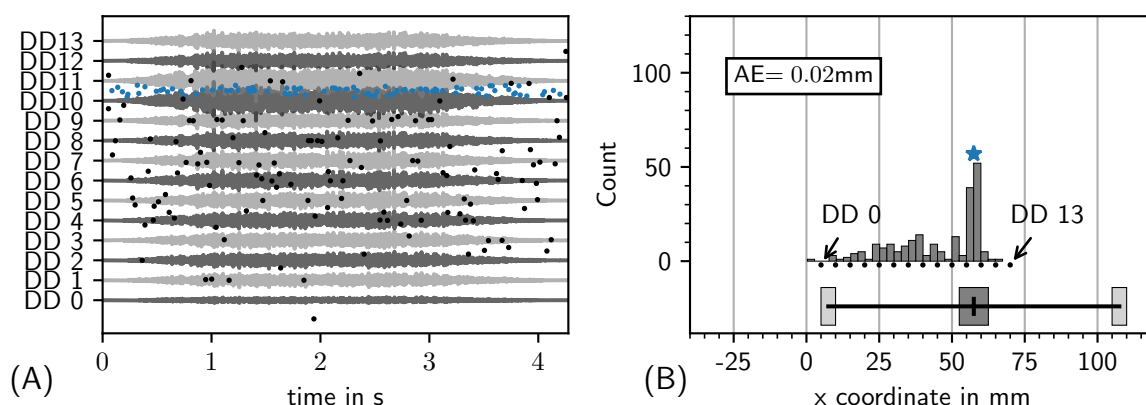


Figure 5: In (A) all 14 simulated double differential EMG signals for one of the six virtual muscles for one of the six virtual muscles is displayed. Blue dots mark the innervation zone location estimates of an innervation zone center cluster. The black dots are innervation zone estimates, which are not part of a cluster. In (B) the distribution of innervation zone estimates is shown. The blue asterisk marks the position of the innervation zone cluster center. In the lower part of the plot, the actual innervation zone region and the myotendinous junction regions are displayed in the same style as in fig. 3. The absolute error from the cluster center (blue asterisk) and the actual innervation zone center is shown at the top. The absolute error in this case is below 1% of the inter electrode distance.

chance that motor unit potentials, which are only partly within the window, are tracked during Step 1 of the innervation zone center estimation. The window was shifted over the EMG signals in 20ms steps, resulting in 20ms overlaps. The window width as well as the window overlap was chosen after inspection of the motor unit potentials.

For each window, an innervation zone center was estimated as described above. Second, under the assumption of an isometric contraction, these estimated positions are clustered in the position domain (axis of the electrode array) using DBSCAN (Pedregosa et al., 2011). This leads to an estimate of possible multiple innervation zone locations per simulation experiment. The innervation zone center estimation was parameterized with $\text{eps} = 0.1$ and $\text{min_samples} = 10$. Per simulation setup presented in fig. 3 the innervation zone clusters were identified and compared to the ground truth, i.e. the center of all innervation point locations.

3 RESULTS

As described, two scenarios with three parameter sets each were simulated, resulting in six simulated EMGs (virtual muscles). The input for each simulation was a common drive (CD) signal in a trapezoidal shape as displayed in fig. 4 and as depicted as inset in fig. 1. For all six simulated EMG signals, the extended version of the innervation zone estimation algorithm was applied as described in section 2.3. For one arbitrarily selected of the six virtual muscles a detailed view on the estimated innervation zones is shown in fig. 5.

In fig. 5 (A) the whole simulated EMG signal is displayed with the estimated innervation zone centers for all time windows. The innervation zone estimates that are part of the accepted cluster are displayed as blue dots. The rejected innervation zone estimates are displayed in black. In fig. 5 (B) the distribution of innervation zone estimates (compared with (A)) over the double differential electrode positions is shown, as well as the center of the accepted cluster (blue asterisk). There is a noticeable accumulation of innervation zone centers in the middle of the array. The accepted innervation zone center is near the maximum in the histogram and close to the actual innervation zone center of the simulated muscle ($\text{AE} = 0.02 \text{ mm}$).

For all simulated virtual muscles, the innervation zone distribution over the electrodes and the accepted cluster center are shown in fig. 6. In general, all the accepted clusters of innervation zone estimates are close to the actual innervation zone locations. For all clusters, the difference between their mean estimate and the actual innervation zone center is below 1 mm. In case of those virtual muscles with their innervation zone center close to the middle of the array (2. column in fig. 6) the error becomes minimal (0.05 mm and 0.08 mm) for both scenarios. The worst value for the estimation accuracy is 0.56 mm.

In case of the simulations where the innervation zone is close to the end of the array, there seem to be clusters of false estimates in the middle of the electrode array.

In general, the mean absolute error is $\text{MAE} = 0.19 \text{ mm}$ ($\text{SD}(\text{AE}) = 0.19 \text{ mm}$).

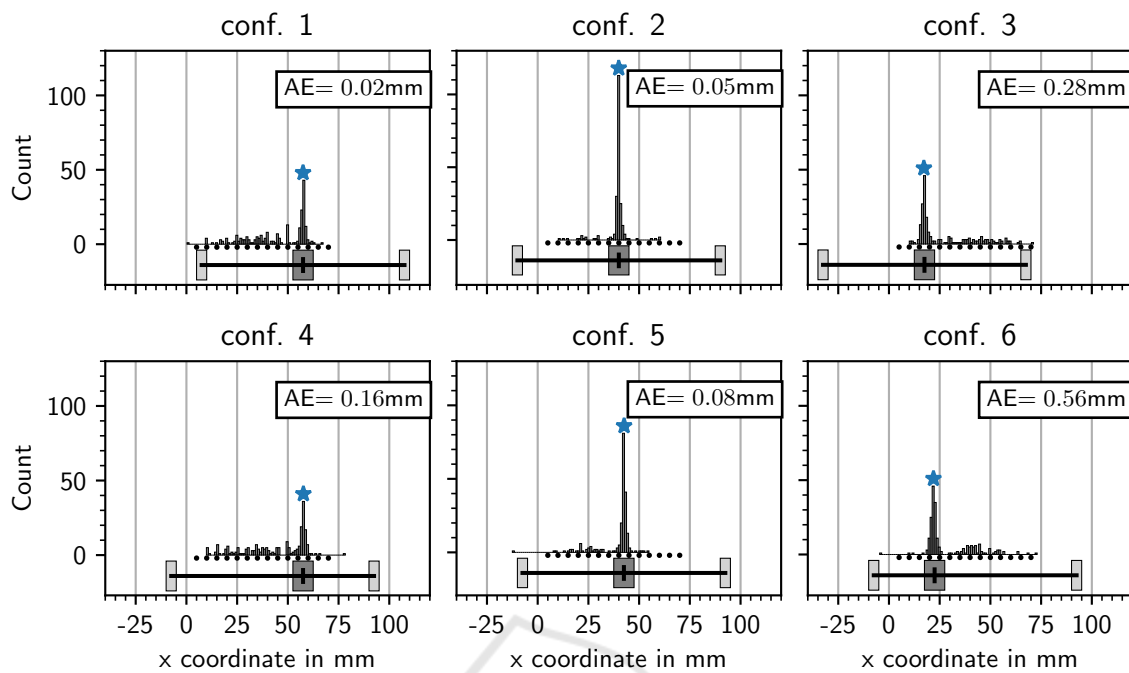


Figure 6: Depiction of the innervation zone location estimate distributions for all six simulated virtual muscles are shown in the same style as in fig. 5 (B). The blue asterisk marks the center of the accepted innervation zone cluster. All absolute errors between the cluster centers and the actual innervation zone centers are below 1 mm.

4 DISCUSSION AND CONCLUSION

This study shows that the newly proposed algorithm for the innervation zone center estimation can be used for continuous EMG signals by segmenting the EMG in overlapping windows. Even with this straight forward approach of segmenting the EMG data, a considerably good result was achieved, since the absolute prediction error was below 0.57 mm for all tested configurations (MAE = 0.19 mm, SD(AE) = 0.19 mm). The mean absolute error is 3.8 % of the inter electrode distance 5 mm. This is a result that is close to another recently published innervation zone estimation algorithm (Huang et al., 2023). Huang et al. report for their principal component based algorithm a mean difference of 3 % (up to 8 % depending on the experiment conditions) of the inter electrode distance, that is 8 mm in their setup. For an extensive comparison, the two algorithms would have to be evaluated with the same dataset.

A further result of the investigation was that the prediction error of the algorithm varies with the electrode array location relative to the innervation zone. When the electrode array was placed above the innervation zone, a prediction error of $AE \leq 0.05$ mm was achieved. Next steps will include the investigation of

the dependency between the prediction error and different electrode configurations as well as the derivation of a model which is also able to follow the movement of the innervation zone under different contraction scenarios of a muscle (e.g. isometric, isotonic and auxotonic conditions).

ACKNOWLEDGEMENTS

This work has been supported by the research training group “Dateninja” (Trustworthy AI for Seamless Problem Solving: Next Generation Intelligence Joins Robust Data Analysis) and by the “TransCareTech” project (Transformation in Care & Technology), both funded by the German federal state of North Rhine-Westfalia. It was also supported by a Career@Bi grant of the University of Applied Sciences and Arts, Bielefeld, Germany.

REFERENCES

- Barbero, M., Merletti, R., and Rainoldi, A. (2012). *Atlas of muscle innervation zones: understanding surface electromyography and its applications*. Springer Science & Business Media.

Beck, T. W., DeFreitas, J. M., and Stock, M. S. (2012). Accuracy of three different techniques for automatically estimating innervation zone location. *Computer methods and programs in biomedicine*, 105(1):13–21.

Farina, D., Fortunato, E., and Merletti, R. (2000). Non-invasive estimation of motor unit conduction velocity distribution using linear electrode arrays. *IEEE Transactions on Biomedical Engineering*, 47(3):380–388.

Fuglevand, A. J., Winter, D. A., and Patla, A. E. (1993). Models of recruitment and rate coding organization in motor-unit pools. *Journal of neurophysiology*, 70(6):2470–2488.

Guzmán, R. A., Silvestre, R. A., Arriagada, D. A., GUZMÁN, R., SILVESTRE, R., and ARRIAGADA, D. (2011). Biceps brachii muscle innervation zone location in healthy subjects using high-density surface electromyography. *int J Morphol*, 29(2):347–52.

Huang, C., Chen, M., Zhang, Y., Li, S., Klein, C. S., and Zhou, P. (2023). A novel muscle innervation zone estimation method using monopolar high density surface electromyography. *IEEE Transactions on Neural Systems and Rehabilitation Engineering*, 31:22–30.

Marateb, H. R., Farahi, M., Rojas, M., Mañanas, M. A., and Farina, D. (2016). Detection of multiple innervation zones from multi-channel surface emg recordings with low signal-to-noise ratio using graph-cut segmentation. *PLoS One*, 11(12):e0167954.

Martin, S. and MacIsaac, D. (2006). Innervation zone shift with changes in joint angle in the brachial biceps. *Journal of Electromyography and Kinesiology*, 16(2):144–148.

Mechtenberg, M. (2023a). UAS-Embedded-Systems-Biomechanics/EMG-concentrated-current-sources: v0.2.2.

Mechtenberg, M. (2023b). UAS-Embedded-Systems-Biomechanics/sEMG-innervation-zone-estimation.

Mechtenberg, M. and Schneider, A. (2023). A method for the estimation of a motor unit innervation zone center position evaluated with a computational semg model. *Frontiers in Neurobotics*, 17.

Mesin, L., Gazzoni, M., and Merletti, R. (2009). Automatic localisation of innervation zones: a simulation study of the external anal sphincter. *Journal of Electromyography and Kinesiology*, 19(6):e413–e421.

Pedregosa, F., Varoquaux, G., Gramfort, A., Michel, V., Thirion, B., Grisel, O., Blondel, M., Prettenhofer, P., Weiss, R., Dubourg, V., Vanderplas, J., Passos, A., Cournapeau, D., Brucher, M., Perrot, M., and Duchesnay, E. (2011). Scikit-learn: Machine learning in Python. *Journal of Machine Learning Research*, 12:2825–2830.

Petersen, E. and Rostalski, P. (2019). A comprehensive mathematical model of motor unit pool organization, surface electromyography, and force generation. *Frontiers in physiology*, 10:176.

Piitulainen, H., Rantalainen, T., Linnamo, V., Komi, P., and Avela, J. (2009). Innervation zone shift at different levels of isometric contraction in the biceps brachii

muscle. *Journal of electromyography and kinesiology*, 19(4):667–675.

Zhang, C., Peng, Y., Li, S., Zhou, P., Munoz, A., Tang, D., and Zhang, Y. (2016). Spatial characterization of innervation zones under electrically elicited m-wave. In *2016 38th Annual International Conference of the IEEE Engineering in Medicine and Biology Society (EMBC)*, pages 121–124. IEEE.

APPENDIX

Table 1: List of constant parameters for the EMG simulation experiments.

Parameter	Value	Reference
electrode y	0cm	estimated
electrode z	2cm	estimated
W_I	1cm	estimated
W_{TL}	0.5cm	estimated
W_{TR}	0.5cm	estimated
R	$\sqrt{\frac{10\text{cm}^2}{\pi}}$	estimated
$P_{IZ,y}$	0cm	estimated
$P_{IZ,z}$	0cm	estimated
N_{MU}	774	(Mechtenberg and Schneider, 2023)
C_1	20	(Petersen and Rostalski, 2019)
C_2	1.5	(Petersen and Rostalski, 2019)
C_3	30	(Petersen and Rostalski, 2019)
C_4	13	(Petersen and Rostalski, 2019)
C_5	8	(Petersen and Rostalski, 2019)
C_6	8	(Petersen and Rostalski, 2019)
C_7	0.05	(Petersen and Rostalski, 2019)